A Numerical Study of the Flow through a Safety Butterfly Valve in a Hydro-Electric Power Scheme

A. D. Henderson[1], J. E. Sargison[1], G. J. Walker[1] and J. Haynes[2]

[1] School of Engineering, University of Tasmania, Hobart, 7001 AUSTRALIA

[2] Zinifex Ltd, Lutana, Tasmania, 7009 AUSTRALIA

Abstract

A numerical study of the flow through a safety butterfly valve used in a hydro-electric power scheme to stop water supply to a downstream penstock is reported. Computational fluid dynamics applied in a quasi-steady manner is used to predict the hydrodynamic torque versus opening angle characteristic during a constant head test. Factors influencing these results, such as Reynolds number and unsteady flow effects, are found to be significant. The predicted results are compared with field measurements of the full-size valve. Issues associated with applying the numerical results to predict valve characteristics at higher Reynolds numbers are discussed. Further computational and experimental studies are recommended.

Introduction

Hydro-electric power schemes require safety valves to stop water flow from the reservoir to the turbine. Turbines that operate under significant head and have a long penstock tunnel usually need a valve near the upstream reservoir to isolate flow to the penstock tunnel. Butterfly valves are often chosen for this purpose since they have a simple mechanical construction, fast closing time, and more importantly, give a low head loss when fully open (see [7, 8]). The size of these 'hill-top valves' will depend on the size of the section of penstock in which they are housed. Larger valves may have diameters up to 5 m.

The valve investigated in this study is installed in a hydro-electric power generating scheme located in central Tasmania, Australia. The valve has a diameter of $D = 3.048$ m and a leaf of convex cross-section. The valve closing mechanism is similar to that described by Ellis and Mualla [6]. The valve is normally in a fully open position. When the valve is triggered by either an abnormally high flow rate, or a remote controlled signal, a locking mechanism disengages. The valve is then subjected to a large out of balance moment imposed by large weights that act to close the valve. The closing motion of the valve is regulated using two large oil-filled dashpots. Oil is forced from the dashpot chambers through a small orifice, which gives a smooth and near constant valve closing rate. During a valve closure test, the dashpot pressure, valve position, upstream static head and downstream static head are recorded. The torque acting on the valve is then estimated from the measured pressure and the mechanical arrangement of the valve.

The torque acting on a closing valve may be resolved into several components (see American Water Works Association (AWWA) [1]). This may be written as

$$T_t = T_b + T_{cg} + T_d + T_p + T_h \tag{1}$$

where T_b is bearing torque, T_{cg} is torque imposed by an offset centre of gravity of the valve, T_d is hydrodynamic torque, T_p is the torque due to packing torque, and T_h is torque due to hydrostatic pressure. The sign convention used in this study is for torque to be positive when acting in the closing direction.

Components T_b and T_p always act in the opposite direction to the valve closing direction. Components T_d and T_{cg} will depend on the valve geometry, and may act in the either direction [1, 6].

It is common to express the hydrodynamic torque T_d in the form of a dimensionless torque coefficient. The two most common definitions are

$$C_{t_1} = \frac{T_d}{(\frac{1}{2}\rho \bar{u}^2)D^3} \tag{2}$$

and

$$C_{t_2} = \frac{T_d}{(\Delta P)D^3} \tag{3}$$

where ΔP represents the static pressure differential across the valve. AWWA [1] suggests for model testing, that the downstream pressure should be measured at least $10D$ downstream to allow for sufficient pressure recovery and the upstream pressure should be measured at least $2D$ upstream.

Solliec and Danborn [15] compared torque coefficient results presented as Eq. (2) and Eq. (3) and found Eq. (2) to be less sensitive to effects of other system losses such as bends and elbows, and thus more useful definition for comparing valve torque characteristics for different valves. Eq. (3), however, is the more commonly used or 'classic' approach, and will be used in this study since flow rate information was not available in the experimental field data.

A common method of determining the valve torque characteristic of a butterfly valve is by a constant head test as described in AWWA [1]. In that test, the valve is positioned in a long horizontal section of pipe that is fed by a constant head source. Measurements of torque and head loss are then made at various valve angles. The dynamic pressure reduces as the valve is closed, which can give very high values of C_{t_1} at high valve angles ($\alpha > 65°$). However, maximum hydrodynamic torque occurs at much lower angles and is better reflected by Eq. (3) as the static pressure does not vary significantly during the test.

The actual head-flow characteristic will differ from that in such simple model tests because there will be greater operating head, additional head loss components due to penstock friction, bends and transitions; and also a head drop across the turbine. In an actual test the turbine head reduces as the valve closes, leading to very low pressure behind the valve. To prevent damage to the penstock tunnel, anti-vacuum valves located a short distance downstream from the valve admit air into the penstock tunnel when the pressure drops below atmospheric. Admitting air into the tunnel may also assist in reducing the extent of cavitation [1]. Owing to these factors, the maximum hydrodynamic torque will occur at a greater valve angle than predicted in a constant head test. Nonetheless, the dimensionless torque coefficient should only differ due to departure from similarity conditions. Numerous studies involving model testing of butterfly valves [12, 7, 5, 15] show that the hydrodynamic torque coefficient approaches a constant value at high Reynolds number.

AWWA [1] recommends a minimum Reynolds number Re_D for model testing of 10^5.

This study uses ANSYS CFX 11 software to predict the hydrodynamic torque acting on a butterfly valve. The aim is to establish an accurate model for predicting the valve loads and torques that would occur in the event of a penstock burst or turbine failure, as the increased flow rate would lead to increased hydrodynamic forces and moment acting on the valve.

Nomenclature

C_{t_1}	torque coefficient defn 1 $= T/(\rho \bar{u}^2 D^3)$ [-]
C_{t_2}	torque coefficient defn 2 $= T/((\Delta P)D^3)$ [-]
D	diameter of valve and housing $= 2R$ [m]
L_e	entry length [m]
P	pressure [Pa]
T	torque [Nm]
T_b	bearing torque [Nm]
T_{cg}	torque due to offset centre of gravity [Nm]
T_d	hydrodynamic torque [Nm]
T_h	hydrostatic torque [Nm]
T_p	packing torque [Nm]
u	velocity [m/s]
$\bar{u}$	mean velocity $= Q/\pi R^2$ [m/s]
u^*	friction velocity $= \sqrt{\tau_w/\rho}$ [m/s]
u_{max}	local maximum velocity [m/s]
Q	volumetric flow rate [m³/s]
r	radial distance from penstock centreline [m]
R	radius of valve and housing [m]
X	penstock distance from valve centre [m]
X'	major axis of valve leaf section [m]
y	wall normal coordinate [m]
y^+	dimensionless normal distance from wall $= yu^*/\nu$ [-]
Y	upward distance from penstock centre [m]
Y'	minor axis of valve leaf section [m]
Re_D	Reynolds number $= \rho \bar{u} D/\mu$ [-]
Z	axial coordinate of valve [m]
μ	dynamic viscosity of water [Pa.s]
ν	kinematic viscosity of water [m²/s]
ρ	density of water [kg/m³]
τ_w	wall shear stress [Pa]
α	valve angle relative to open position [°]

Scope of Investigation

Valve Geometry

A schematic diagram of the valve geometry at mid-section is shown in Figure 1. The valve is symmetrical about the $Y' - Z$ and $X' - Z$ planes and maintains a uniform maximum leaf-section thickness t of 510 mm along much of its axis. A small tip gap of 4 mm is sealed by a circular rubber seal. Other details of the valve geometry were provided by Barnbaum [3].
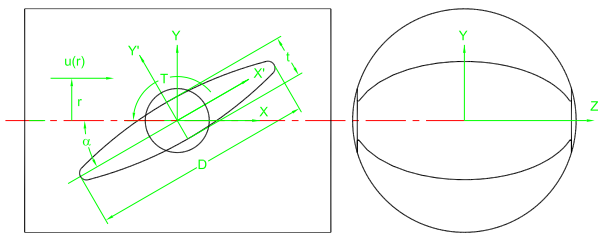

Figure 1: Butterfly valve arrangement

Flow Conditions

The valve is situated in a long straight circular section of steel pipeline. Two flow rate cases were selected to match the experimental field measurements available: Cases A and B shown in Table 1.

Case	Q (m³/s)	Re_D (10^6)	$\bar{u}$ (m/s)
A	21.2	8.8	2.91
B	35.3	14.7	4.84

Table 1: Flow conditions

Numerical Model

A quasi-steady modelling approach was used in this study, where steady flow solutions were obtained at various valve angles. This was deemed to be acceptable given the long valve closing time of 6 minutes relative to the flow transit time. The valve tip speed at mid-plane was at least 2 orders of magnitude lower than the upstream flow speed $\bar{u}$ for the higher flow rate in Case B. However, the velocity around the valve tip is considerably faster than in the upstream flow.

It was recognised that the system does not respond instantly to a change in flow conditions, as it takes approximately 5 seconds for pressure waves to traverse the entire length of penstock. Dynamic effects would become significant at high valve angles where the rate of reduction in flow rate with time becomes large. The experimental results provided by Barnbaum [4] showed evidence of this by a surge in upstream head at around $\alpha = 60°$.

The valve geometry was created using SolidEdge software and imported into ANSYS Design Modeller. A rubber seal around the rim of the valve was not included in the model to avoid problems associated with meshing very small sliver volumes. The gap closed by the seal is small ($0.003R$) and was not expected to have a significant influence on the flow through the valve. The flow was assumed to be symmetrical about the valve $X - Y$ centreplane, and thus only half of the flow field was modelled by applying a symmetry boundary condition. Further details of the geometry creation are given in Haynes [9].

The modelling aimed to simulate a constant head test commonly used to determine valve characteristics [1]. Since defining a velocity profile at the model inlet would set the flow rate and the head loss across the valve, it was decided to instead model a long upstream section of penstock and specify the total pressure at inlet, thereby allowing the velocity profile to develop before reaching the valve. This distance required for the flow to develop may be estimated using an empirical formula for entry length given by Munson [13] as $L_e/D = 4.4(Re_D)^{1/6}$. This correlation predicts lengths of approximately $56D$ and $60D$ for Cases A and B respectively. Following this it was decided to make the upstream section of penstock $60D$ upstream from the valve axis and the downstream section $15D$ downstream from the valve axis.

The total pressure at inlet was set to give the desired flow rate at fully open condition ($\alpha = 0°$) and this was then maintained for solutions at other valve angles, thereby allowing the flow rate to decrease accordingly with the head loss imposed by the valve.

The computational domain was divided into three main sections: upstream penstock, near valve section, and the downstream penstock. Upstream and downstream penstock sections were meshed using an inflated layer of hexahedral elements on the walls, with triangular-based prism elements in the centre. A

layer of inflated elements was used on the valve face to improve modelling of the boundary layer. The surrounding mesh consisted of tetrahedral elements. Meshes were generated for valve angles between $0°$ and $80°$ in steps of $10°$. The total number of elements contained in each mesh varied between 2.2×10^6 and 2.8×10^6. Figure 2 shows the mesh on the valve symmetry plane at a valve angle of $\alpha = 60°$.
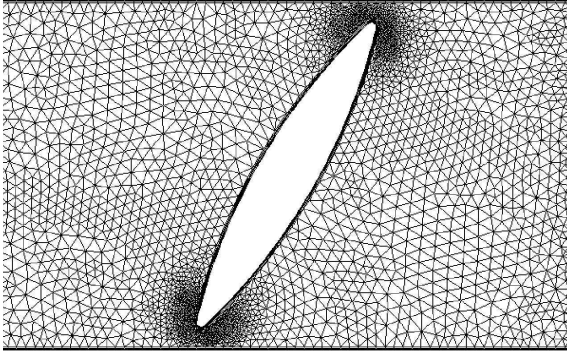

Figure 2: CFD mesh on the *X-Y* symmetry plane for a valve angle of $\alpha = 60°$

The Shear Stress Transport (SST) turbulence model was used for turbulent closure as it is well regarded in prediction of flow separation in an adverse pressure gradient [2]. Studies of Lin and Schohl [11] and Leutwyler and Dalton [10] found that the SST model produced best agreement with experimental measurements of hydrodynamic loading and torques acting on butterfly valves.

The near wall flow was modelled using 'automatic' wall functions, which automatically switch between a low Reynolds number approach to scalable wall functions depending on local conditions and the wall normal element spacing [2]. This effectively removes the lower limit of y^+ required by standard wall functions. The y^+ values of the mesh varied with both inlet Reynolds number and valve angle, but were mostly less than 200, which is within the specifications given in the software documentation [2]. A high resolution discretisation scheme was used (see [2]). The six equations solved were u, v and w-momentum equations, and conservation of mass, turbulent kinetic energy (k) and turbulent frequency (ω).

A convergence criterion for maximum RMS residual of 10^{-6} was set, which is two orders of magnitude below the default level used by the solver [2]. Solution times were generally around $15-20$ hours using 4 processors of a SGI ALTIX 4700 system (Itanium 2, 1.6 GHz). An automatic time-scale with a conservative length scale and time factor of 0.25 was used to improve stability at the expense of a slightly longer solution time.

Results

Convergence

Table 2 shows the maximum RMS residuals obtained for each of the steady flow solutions. Note that a value of 1.0×10^{-4} is the default level for the solver. Acceptable convergence level was achieved in all cases except $\alpha = 20°$ and $\alpha = 30°$. Oscillations were observed in the residuals for those cases, which can be indicative of unsteady flow behaviour. Those cases were restarted as transient simulations and the residuals then reduced to the target convergence criterion.

Valve Angle (°)	Case A (10^{-4})	Case B (10^{-4})
0	0.01	0.01
10	0.01	0.01
20	43	26
30	38	31
40	1.4	1.6
50	0.10	0.08
60	0.01	0.01
70	0.03	0.03
80	1.50	0.91

Table 2: Maximum RMS convergence residuals for steady flow solutions

Inlet Velocity Profile

The upstream velocity profile was compared against the standard 'power law' to verify that the flow had developed by the time it reached the valve. The power law may be expressed as

$$\frac{u}{u_{max}} = \left(1 - \frac{r}{R}\right)^{1/n} \quad (4)$$

where the index n was determined by applying a curve fit to the predicted velocity profile. These were determined as 10.5 and 11.4 for Cases A and B respectively. Schlichting [14] used this approach to determine indices for smooth pipe flow data at lower Reynolds numbers than those considered in this study. Predicting the index n by extrapolating the experimental results to the higher Reynolds numbers given in Table 1 yields similar results of 10.8 and 11.2 for Cases A and B respectively.
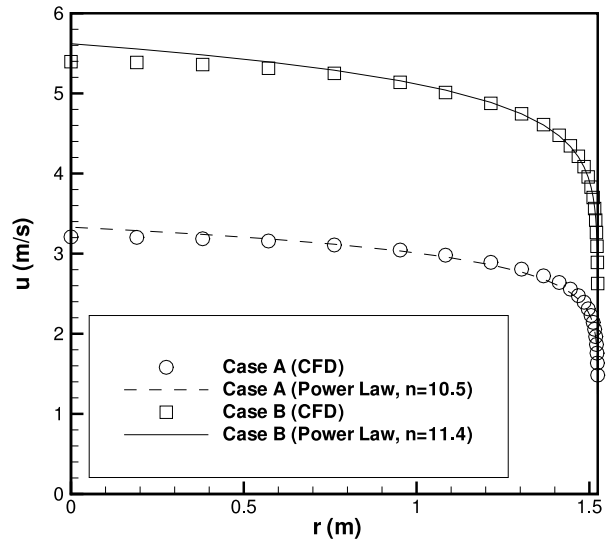

Figure 3: Velocity distribution $2.1D$ upstream from the valve axis ($\alpha = 0°$)

Figure 3 compares the predicted velocity profile from the CFD and power law at a location $2.1D$ axially upstream from the valve shaft axis for $\alpha = 0°$. Reasonable agreement is observed in the near-wall region, but this deteriorates slightly toward the centre. It is possible that the flow has not fully developed, although Schlichting [14] shows that the power law becomes increasingly inaccurate towards the centre of the flow ($r/R < 0.2$) and produces an unrealistic velocity gradient at the centre. Further increasing the length of upstream penstock was deemed unnecessary for this study.

The profile was also checked at a distance of $4.2D$ upstream from the valve axis. The maximum difference between profiles was less than $0.02\bar{u}$ which confirms that there was no significant upstream influence of the valve at these positions.

Mesh Resolution

A mesh refinement study was completed for the valve Case B and is shown in Fig. 4. The mesh was coarsened equally in all directions for each subsequent trial. The number of elements in the inflated wall layer was changed to maintain an acceptable aspect ratio. However, the first element height and expansion ratio of the inflated wall layers were not changed to avoid altering the boundary layer modelling.
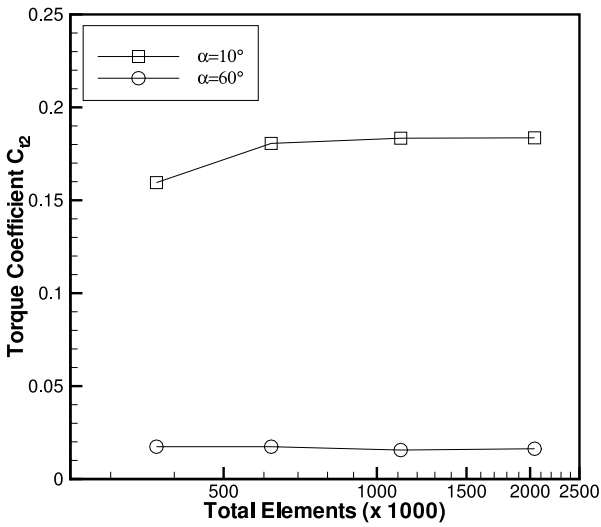
Figure 4: Mesh resolution test for Case A

These results suggest that sufficient resolution was provided by the mesh of around 2×10^6 elements used for the purposes of this study.

Description of Flow Field

A sequence of plots showing the mid-valve flow field on the X-Y symmetry plane for Case B is shown in Fig. 5. The velocity magnitude shown in each plot has been normalised by the local maximum velocity u_{max}. At $\alpha = 10°$, there no separation observed at mid-plane. Although not shown, a small region of separated flow forms behind the valve close to the wall. For $\alpha = 20°$ a small separation forms at mid-plane but the flow appears to reattach. The extent of this separation increases with valve angle, so that most of the downstream valve surface is separated at $\alpha = 40°$. Further increasing the valve angle increases the extent of the downstream flow separation. Despite this, the downstream length of flow domain was sufficiently long to prevent reverse flow at the outlet.

A dominant feature of the downstream flow is a counter-rotating streamwise vortex pair that develops at all non-zero valve angles. Since the valve is at an angle to the upstream flow, the pressure differential across the valve directs fluid downward near the sides, creating a swirling flow. The strong vortical flow persists throughout the whole downstream flow domain. This also implies the existence of a lift force perpendicular to the pipe axis. Visualisations of this secondary flow are shown in Figs 6 and 7.
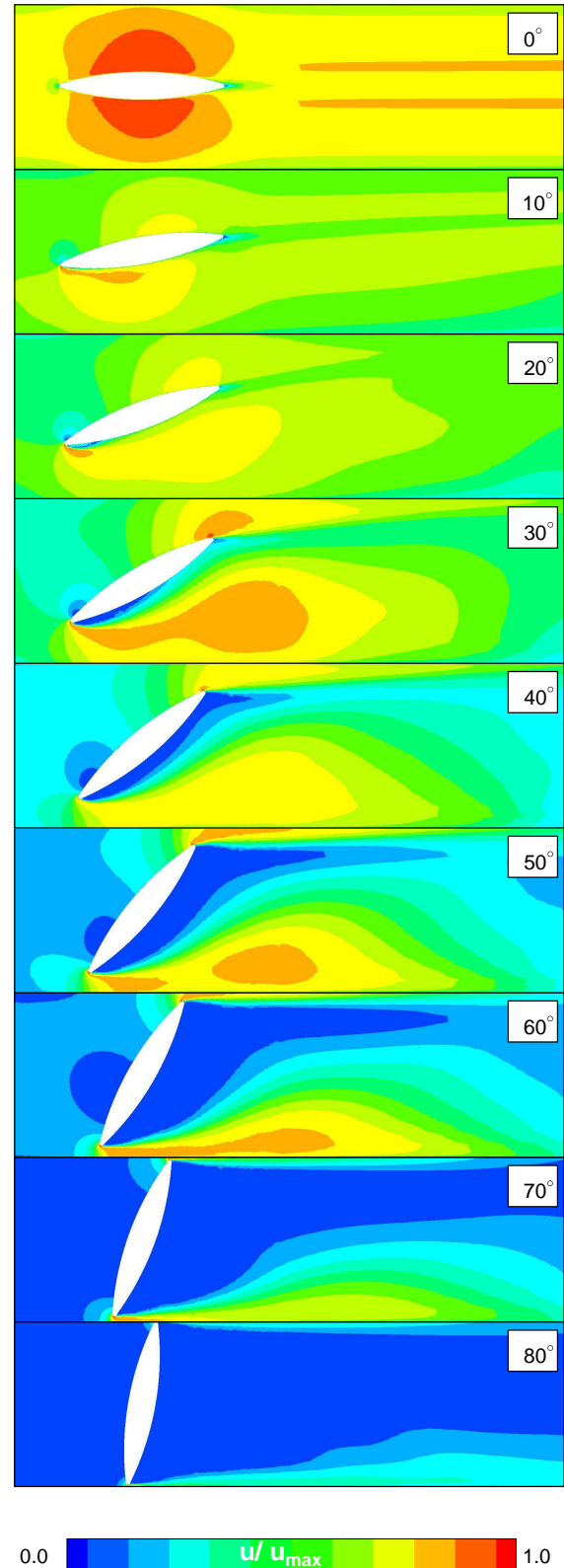

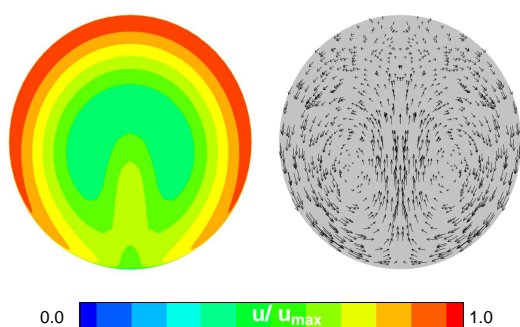Figure 5: Valve flow field on X-Y symmetry plane for Case B.

Figure 6: Contours and velocity vectors on axial plane $4D$ downstream from the valve axis for Case B at $\alpha = 60°$
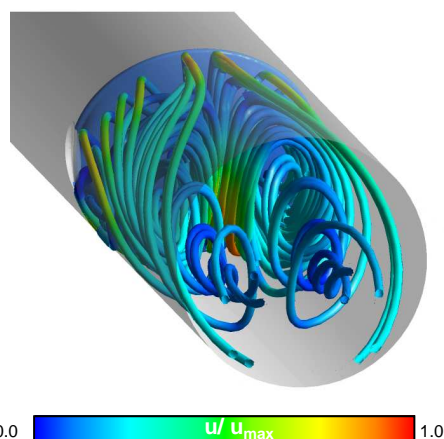

Figure 7: Pathlines $4D$ downstream from the valve axis for Case B at $\alpha = 60°$

Unsteady Flow Effects

The flow behind the valve is known to be unsteady. Leutwyler and Dalton [10] note that for valve angles less than around 70° the flow downstream from the valve is dominated by strong unsteady vortical disturbances. This is caused by flow separation at the leading edge of the downstream face of the disk and the large diffusion of the flow around the downstream side of the valve. The vortical disturbances were reported to cause fluctuations in pressure, force and torque acting on the valve.

At moderate angles, after α is large enough to get flow separation, there will be a bluff body flow. For $\alpha = 30°$, the effective dimension will be about $D/2$ (based on the frontal length of valve leaf on the X-Y symmetry plane). For regular vortex shedding with a Strouhal number of $St = 0.2$ we would expect an eddy shedding frequency of about 1.3 Hz.

Figure 8 shows the torque coefficient from both the transient calculation and poorly converged steady solution (see Table 2). The transient calculation shows oscillations in torque coefficient with a frequency of around 1 Hz, which is similar to that estimated for the eddy shedding of a bluff body of this size. The convergence of the steady solution is clearly hampered by unsteady flow, but it nonetheless reaches a value close to the average estimated in the unsteady flow solution.

Further confirmation of periodic eddy shedding is shown in Fig. 9 which clearly shows an alternating shedding pattern.
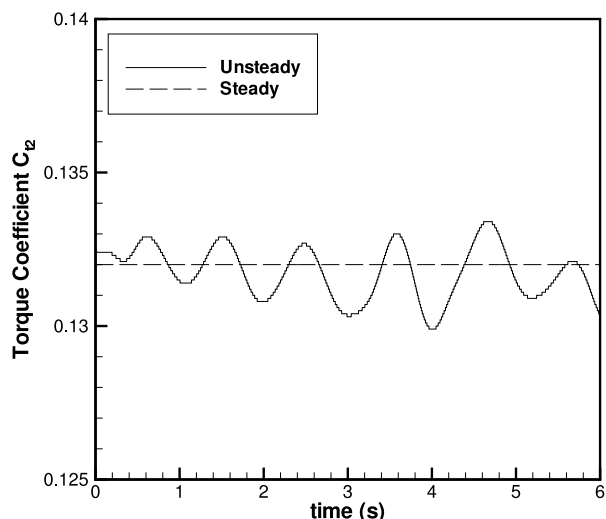

Figure 8: Torque coefficient for transient solution of Case B at $\alpha = 30°$

Reynolds Number Dependence

Solutions over a range of Reynolds numbers were obtained at two valve positions to investigate Reynolds number effects. The results are shown in Fig. 10. The torque coefficient shows some variation even at high Reynolds number. Solliec and Danbon [15] also found torque coefficient measured on a model valve continued to change at a Reynolds number of 7×10^5. It is likely that changes in upstream velocity profile with Reynolds number are a contributing factor.
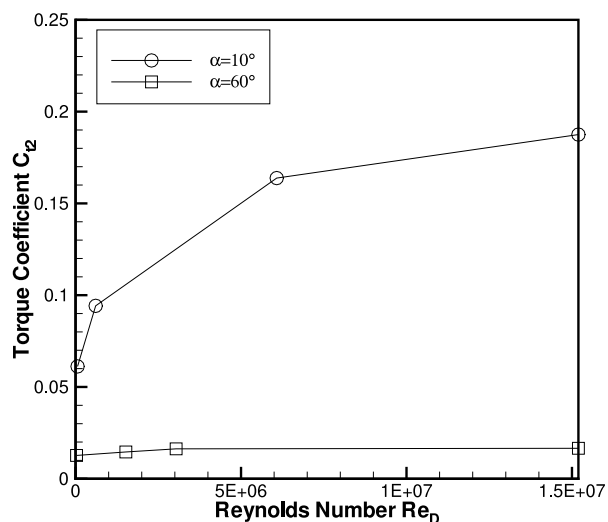

Figure 10: Predicted influence of Reynolds number on torque coefficient C_{t_2}

Comparison with field measurements

Data from valve closure tests were provided by Hydro Tasmania (Barnbaum [4]). In order to determine the hydrodynamic torque component from the total torque estimate, the total torque was corrected using data from a still water test. This approach aimed to remove most of the torque components common to both the still water and flow closure tests. Common components include T_{cg}, T_h, and to some extent T_b and T_p, but additional bearing friction may induced by hydrodynamic loadings and would not
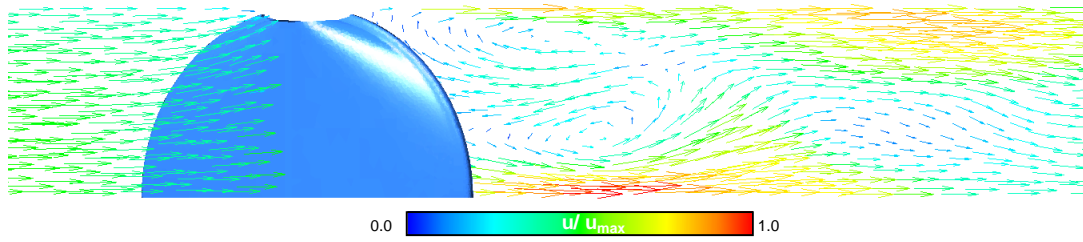
Figure 9: Instantaneous velocity vectors shown on a X-Z plane for Case B at $\alpha = 30°$

be accounted for. The correction was applied using

$$T_d \approx T \left(1 - \frac{P^*}{P} \right) \qquad (5)$$

where T is the torque estimated from the pressure measured in the dashpots, P is the pressure in the dashpots, and P^* is the pressure measured in the dashpots during a still-water test.
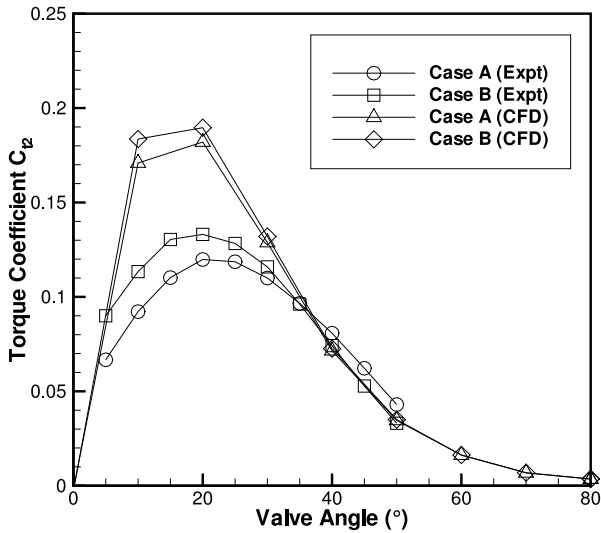

Figure 11: Measured and predicted torque coefficient

Figure 11 compares predicted and measured valve torque characteristics. The curves qualitatively agree in terms of shape and sign, with maximum torque coefficient occurring near $\alpha = 20°$. However the maximum torque from the experimental results is significantly less than predicted. This difference may partially be explained by two main factors. First, there will be viscous friction loss in the oil filled dashpots that is not accounted for in the torque estimation. Second, the bearing friction would be expected to increase as hydrodynamic loading is increased. Both factors would contribute to reduce the indicated experimental torque below the actual experimental torque. Other contributing factors include cavitation, which will alter the flow pattern around the valve, and consequently the torque required to close the valve; and the accuracy of the pressure measuring instrumentation. Bourdon type pressure gauges used to measure the upstream and downstream static head have low resolution and could not be expected to give accurate readings for small changes in pressure.

The CFD results may have been influenced by use of the symmetry boundary condition. For example, use of symmetry plane in the flow about a cylinder will interrupt eddy shedding. Dif-

ferences due to Reynolds number effects will arise from differences between the actual head flow characteristic will be differ from the constant head approximation used in the CFD model.

Conclusions

This study has described a numerical study of the flow though a safety butterfly valve. The numerical results showed that a strong vortical flow pattern develops downstream from the valve, and that the flow becomes unsteady over a range of valve angles. The shape and sign of the predicted torque characteristic agreed with experimental field measurements, although the maximum values differ. The study highlights the need for improved field measurements that include measurement of flow rate. This would enable CFD simulations to be preformed at more representative conditions, possibly including a cavitation model. Unsteady data from a scale model of the valve would also assist in validating the CFD model.

Acknowledgements

References

[1] American Water Works Association (AWWA), Butterfly valves: Torque, head loss and cavitation analysis, Technical Report M49, American Water Works Association, 2001.

[2] ANSYS Europe Ltd, ANSYS CFX solver modeling guide, V11, Technical report, ANSYS Europe Ltd, 2007.

[3] Barnbaum, G., Engineering drawing of 120" butterfly valve, Private communication to J. Haynes, 2006.

[4] Barnbaum, G., Hilltop valve flow closure test report, Private communication to J. Haynes, 2006.

[5] Danbon, F. and Solliec, C., Aerodynamic torque of a butterfly valve— influence of an elbow on time-mean and instantaneous aerodynamic torque, *ASME Journal of Fluids Engineering*, **122**, 2000, 337–344.

[6] Ellis, J. and Mualla, W., Dynamic behaviour of saftey butterfly valves, *Water Power and Dam Construction*, **121**, 1984, 26–31.

[7] Gaden, D., A contribution to the study of butterfly valves. part 1, *Water Power*, **55**, 1951, 456–474.

[8] Gaden, D., A contribution to the study of butterfly valves. part 2, *Water Power*, **56**, 1952, 16–22.

[9] Haynes, J., CFD analysis of the flow past a butterfly valve, Honours thesis, University of Tasmania, 2007.

[10] Leutwyler, Z. and Dalton, C., A computational study of torque and forces due to compressible flow on a butterfly valve disk in mid-stroke position, *ASME Journal of Fluids Engineering*, **128**, 2006, 1074–1088.

[11] Lin, F. and Schohl, G. A., CFD prediction and validation of butterfly valve hydrodynamic forces, in *In Conference Proceedings of World Water and Environmental Resources Congress*, editors G. Sehlke, D. F. Hayes and D. K. Stevens, 27 June – 1 July, Salt Lake City, USA, 2004.

[12] MacLellan, D. A. and Caruthers, J. H., Hydraulic characteristics and limitations of butterfly valves for flow control, in *Glenfield Gazette. Valve Symposium— 'Fluid Control in Industry', London, May 1–3*, 2001, 9pp.

[13] Munson, B. R., Young, D. F. and Okiishi, T. H., *Fundamentals of Fluid Mechanics*, John Wiley Inc, 2002, fourth edition.

[14] Schlichting, H., *Boundary-Layer Theory*, McGraw–Hill, 1968, 6th edition.

[15] Solliec, C. and Danson, F., Aerodynamic torque acting on a butterfly valve. comparison and choice of a torque coefficient, *Journal of Fluids Engineering*, **121**, 1999, 914–917.